Love wave tomography of the United States

Anant Hariharan[1], **Colleen A. Dalton**[1]

[1]Department of Earth, Environmental, and Planetary Sciences, Brown University, Providence, RI, USA

Key Points:

- We describe an approach to eliminate overtone interference and improve the quality of Love wave measurements.
- We present the first earthquake-derived Love wave phase velocity maps of the conterminous U.S., at periods up to and including 75 seconds.
- Our maps require radial anisotropy in many regions of the crust and upper mantle beneath the US.

Corresponding author: Anant Hariharan, anant_hariharan@brown.edu

Abstract

Love wave phase velocity maps provide essential constraints on radial anisotropy and deformation in the crust and upper mantle. However, the phenomenon of overtone interference causes scatter and systematic bias in the velocity measurements and impedes efforts to image small-scale anisotropic variations. We develop an approach for identifying Love wave measurements that are biased by overtone interference, demonstrate its efficacy with EarthScope USArray data, and determine the first earthquake-derived Love wave phase velocity maps for the entire conterminous U.S. in the period range 35-75 s. We show that radial anisotropy in parts of the crust and most of the lithospheric mantle is necessary to reconcile these maps with Rayleigh wave phase velocities. Our results convey the impact and geographic variability of overtone interference, offer an easy-to-implement method to ameliorate this impact, and present high-resolution constraints on radial anisotropy beneath North America.

Plain Language Summary

Measurements of Love wave phase speeds at different frequencies provide unique information that can help understand how the Earth's interior is deforming. These measurements are difficult to make because other seismic waves interfere with the one we are attempting to measure, resulting in low-quality and biased measurements. Here, we calculate the times at which the different waves arrive and use these times to identify and remove measurements impacted by interference. Images of the Earth's interior made using the resulting cleaned data set are less biased and present new information to understand Earth structure in the upper mantle beneath the US. Our images suggest shear waves polarized in vertical and horizontal directions are required to have different speeds.

1 Introduction

As minerals such as olivine undergo finite strain, they develop a crystallographic or lattice-preferred orientation (LPO), which manifests as anisotropy in measurements of seismic wavespeed (Ribe, 1992). Radial seismic anisotropy, which describes a material with transverse isotropy and a vertical axis of symmetry (Babuska & Cara, 1991), causes a difference in the speeds of horizontally (V_{SH}) and vertically polarized (V_{SV}) shear waves. Love and Rayleigh wave phase velocities are strongly sensitive to V_{SH} and V_{SV},

respectively, and provide the best constraints on radial anisotropy in the lithosphere and asthenosphere. Global studies and those focused on the Pacific basin agree reasonably well on the long-wavelength variations in radial anisotropy and have found, for example, that anisotropy can be attributed to both ridge corner flow and shear between the lithosphere and asthenosphere (Eddy et al., 2022), and that a mismatch between observed radial anisotropy and that predicted by geodynamic models of mantle flow implies the presence of small-scale convection in the deeper asthenosphere ($\approx$ 250 km) (Becker et al., 2008).

Much less is known about smaller-scale variations in radial anisotropy, especially in the continental upper mantle, where radial anisotropy is useful for mapping the degree of crustal extension (Moschetti et al., 2010) and may explain a mid-lithospheric discontinuity observed by scattered body waves (Selway et al., 2015; Karato & Park, 2018). A comparison of four recent, state-of-the-art models of radial anisotropy beneath North America (Fig. S1) shows significant disagreement in both the amplitudes and patterns of heterogeneity, even between models developed with a similar full-waveform inversion approach. This disagreement suggests a consensus has not yet been reached on the distribution of radially anisotropic heterogeneity in the upper mantle beneath the U.S., precluding using these models to make robust inferences about geodynamic processes. A path forward is to incorporate information from regional earthquake-derived Love wave phase velocity maps, which can offer high resolution at the continental scale but were not used in developing the current generation of models. However, it is challenging to develop these regional-scale Love wave phase velocity maps due to noise on the horizontal components of seismometers (e.g., Rohde et al., 2017; Zürn et al., 2022) and overtone interference (Thatcher & Brune, 1969). In this study, we focus on resolving the latter difficulty.

Overtone interference refers to the presence of higher modes in the time window of a waveform where an operator seeks to measure the phase and amplitude of the fundamental mode (FM). Love waves are particularly vulnerable to overtone interference because the FM Love wave has a similar group velocity to that of the first, and in some cases second and third, overtones at periods less than roughly 120 s (Fig. 1a), particularly for oceanic Earth models. Previous work has demonstrated that overtone interference can introduce bias into Love wave phase velocity measurements by causing phase and amplitude measurements to oscillate about their true value as a function of distance

(Foster, Nettles, & Ekström, 2014; Hariharan et al., 2022). Fig. 1b shows an example of this using amplitude measurements made on two sets of synthetic seismograms calculated using normal-mode summation with MINEOS (Masters et al., 2011); one set includes all modes and the other includes only the FM. Amplitude measurements show a long-wavelength oscillation as a function of epicentral distance only when the higher modes are included in the seismograms. The corresponding oscillation in phase (not shown) has a negligible effect on global-scale inversions for radial anisotropy using measurements from a wide range of epicentral distances (Nettles & Dziewoński, 2011), but when phase velocities are measured using differences in phase at nearby stations, as in wavefront-tracking approaches such as Eikonal or Helmholtz tomography (Lin et al., 2009; Lin & Ritzwoller, 2011), or with the two-station method (Foster, Ekström, & Nettles, 2014), the resulting phase velocity measurements oscillate dramatically about their true value, resulting in error of 10% or more for regional-scale studies (Foster, Nettles, & Ekström, 2014; Hariharan et al., 2022). Furthermore, the phase oscillations are not symmetric but sawtoothed as a function of distance. This asymmetry in phase, when differentiated to produce velocity, causes many Love wave phase velocity measurements to be systematically higher than their true value (Foster, Nettles, & Ekström, 2014). This bias has led phase velocity maps constructed from earthquake-derived Love waves to have systematically higher values than their ambient-noise derived counterparts at the same period (Jin & Gaherty, 2015).

In this study, we introduce a quality control method based on removing paths with similar FM and overtone group arrival times in order to minimize bias due to overtone interference. We demonstrate its effectiveness via three metrics applied to Love wave phase velocity measurements: (1) the elimination of bias toward anomalously high velocity, (2) the suppression of scatter, and (3) the suppression of strong distance-dependent oscillations. Our approach is couched in intuitive physics and easy to implement. We apply it along with wavefront tracking to determine new earthquake-derived Love wave phase velocity maps for the contiguous U.S. With predictions of the V_{SV} model of Shen and Ritzwoller (2016), we test the null hypothesis of isotropy in the North American lithosphere.

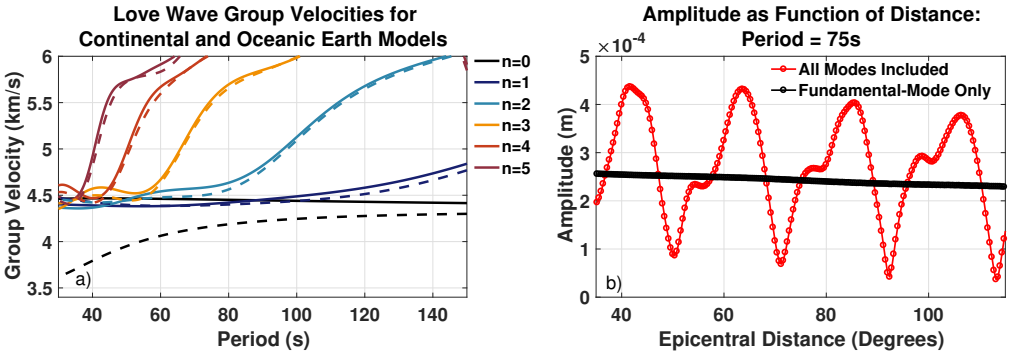

Figure 1. Left: Love wave group velocities for the FM and first five higher modes for continental (dashed line) and oceanic (solid line) Earth models. The continental Earth model is STW105-C (Hariharan et al., 2022) and the oceanic Earth model is ATL2a (James et al., 2014). Right: Love wave amplitudes measured using Fourier analysis on seismograms including all modes (red) and including only the FM (black) at a period of 75 s. The source mechanism for the synthetic seismograms is a strike-slip fault at a depth of 12 km.

2 Data and Methods

2.1 Measurements of Love Wave Phase Velocities

We use Eikonal tomography (Lin et al., 2009) to generate maps of Love wave phase velocity for individual earthquakes. We use a data set of Love wave phase delays observed at EarthScope USArray stations (Eddy & Ekström, 2014, 2020), which contains 1100-1600 teleseismic events at each period and was measured with the approach of Ekström et al. (1997). The event-specific maps are obtained through several pre-processing steps broadly described by Babikoff and Dalton (2019) and specifically outlined in text S1. The final map at any period is calculated by taking the median from all the individual event-based phase velocity maps.

2.2 Description of Our Quality-Control Scheme

We use the difference between the predicted group arrival times of the FM and the first overtone as a proxy for the strength of overtone interference in any phase velocity measurement. We henceforth refer to this value as ΔT.

Predicting group arrival times requires globally defined maps of group speed, which have not been published for Love wave overtones. We therefore calculate global group

velocity maps for the FM and the first overtone using an *a priori* model of 3-D Earth structure. To generate a global Earth model for this calculation we overlay the crustal model CRUST1.0 (Laske et al., 2013) on the mantle model S362ANI (Kustowski et al., 2008). Depth-dependent profiles are then sampled on an evenly spaced grid and provided as input to MINEOS (Masters et al., 2011) to calculate group velocities for the Love wave FM and first overtone. For every period, the location-specific calculations are combined to form group velocity maps, which are used to predict group arrival times for every path in our data set by integrating along the great-circle path from source to receiver. Our predicted FM group velocity maps agree well with the measured GDM52 maps (Ekström, 2011), with an average unsigned difference of less than 0.15 km/s and a correlation coefficient greater than 0.83 at all periods. We calculate ΔT as the first overtone arrival time subtracted from the FM arrival time; thus, most ΔT values are positive. This yields a ΔT value for every phase velocity measurement for every event in the data set.

3 Results: Application of Quality Control to Love Wave Phase Velocity Measurements

In this section, we demonstrate that selecting high-quality Love wave phase velocity measurements on the basis of their ΔT value reduces the negative impacts of overtone interference. As discussed in Section 1, we are concerned with three distinct consequences of overtone interference on Love wave phase velocity measurements: 1) a bias to anomalously high values, 2) increased scatter, and 3) a strong oscillatory distance dependence. To investigate how these consequences are affected by data selection by ΔT, we define measurement error relative to the GDM52 global phase velocity maps (Ekström, 2011); we consider GDM52 to be a smoothly varying reference that is largely unbiased by overtone interference since it was built from phase measurements integrated over long propagation paths. Error for event i in pixel j is calculated as $E_{ij} = c_{ij}^{obs} - c_j^{GDM52}$, where c_{ij}^{obs} refers to the observed event-specific Eikonal phase velocity maps. In the presence of overtone interference, we expect E_{ij} to 1) be systematically greater than zero (Foster, Nettles, & Ekström, 2014), 2) exhibit greater scatter than if no overtone interference is present, and 3) show an oscillatory dependence on epicentral distance.

Every error value has a corresponding ΔT value. In Fig. 2a we bin error by ΔT and plot the median error in each bin. Fig. 2a shows that phase velocity measurements corresponding to lower ΔT values are biased high relative to the reference value. The

median bias at low ΔT is 60-80 m/s (1.5-2.0%), meaning that half of the measurements suffer an even larger bias. However, the median bias decreases noticeably for measurements with larger ΔT values and approaches zero bias for most periods as ΔT approaches the period of interest. Fig. 2b shows that retaining measurements with large ΔT values also reduces the standard deviation of the error in Love wave phase velocities, which is a measure of the amount of scatter in the measurements.

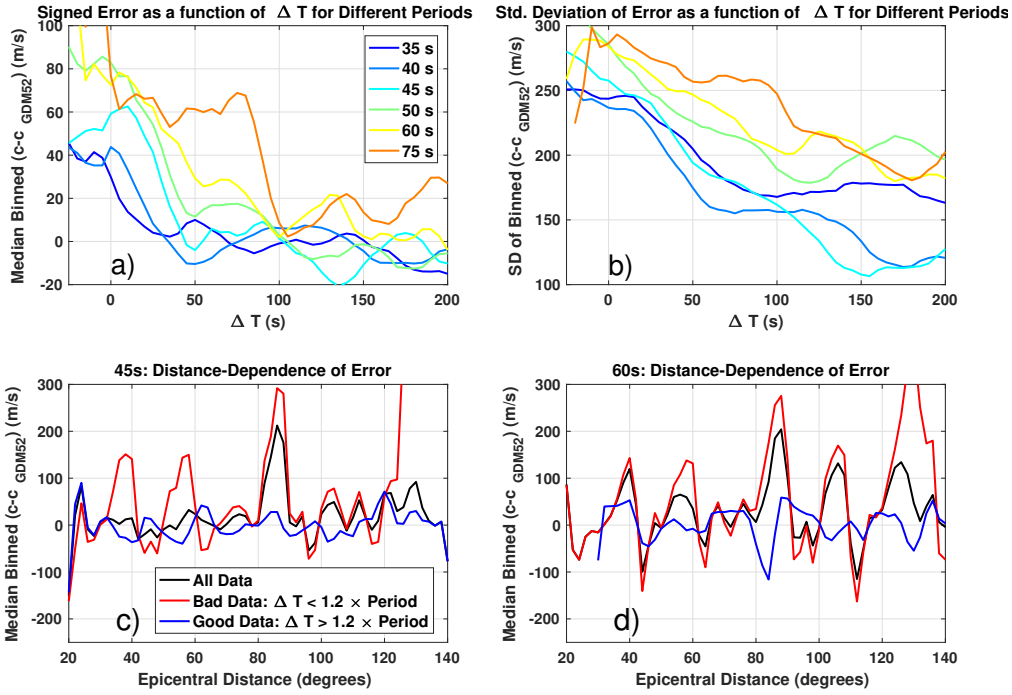

Figure 2. a) Median signed errors in USArray Love wave phase velocities with respect to the GDM52 maps, binned as a function of ΔT, which is the difference in the group arrival times of the FM and first overtone. b) Standard deviation in the errors in USArray Love wave phase velocities with respect to the GDM52 maps, binned as a function of ΔT c) Distance dependence of phase velocity measurements for period=45 s. Blue line: Only using data that pass our quality control criteria. Red line: Only using data that fail our quality control criteria. Black line: All data. d) As in (c) but for period=60 s.

We find that the signed error at low ΔT is consistently larger at longer periods (Fig. 2a). The ΔT value only measures the separation between the peak of the FM and overtone group envelopes, not the wavepackets themselves. At longer periods, these wavepackets by definition take up more space in the time domain; thus, a larger ΔT is required at longer periods to fully separate the two wavepackets. To account for the effect of wavepacket

size, we scale ΔT by the period of the waveform when choosing a threshold to isolate good measurements. We find that retaining the subset of phase velocity measurements for which $\Delta T \geq 1.2 \times period$ (e.g., $\Delta T \geq 54$ s for period=45 s and $\Delta T \geq 72$ s for period=60 s) results in a quality-controlled data set with median signed error less than 15 m/s at all periods, thereby eliminating the majority of the systematic bias while still retaining many measurements. This retains $\approx 43\%$ of the data set at the shortest periods and $\approx 14\%$ at the longest periods. We proceed using this threshold for quality control but note that others may choose differently depending on the size, event distribution, and extent to which overtone interference is present in their data set (Section 5.1).

Importantly, we find that quality control by group arrival time suppresses, and in some cases eliminates, the oscillations in phase velocity measurements as a function of epicentral distance (Fig. 2c,d). When only measurements with ΔT values below the threshold of $1.2 \times period$ are used (i.e., selecting for measurements with strong interference), the measurement error has a clear periodic distance dependence with a wavelength of about 20°. This indicates that our metric is successfully able to identify biased measurements. On the other hand, when only measurements with ΔT values above the threshold are used, the resulting distance dependence is weak at all periods and distances, indicating that our metric is successfully able to isolate good measurements. For the full data set with no selection, the binned values show a strong distance dependence at long periods that grows weaker at shorter periods (Fig. S2).

Finally, in Fig. 3 we show that the quality control approach reduces bias in composite phase velocity maps. We compare maps constructed with and without data selection and find that although the large-scale pattern of heterogeneity is not dramatically affected, the smaller-scale features are altered and the absolute phase velocities can differ by as much as 0.2 km/s in some locations. This is consistent with the bias toward anomalously high velocity that overtone interference induces in phase velocity measurements. Fig. 3 also shows that geographical distribution of data selection is uneven and mostly concentrated in the western U.S., where the impact of overtone interference is more significant (Section 5.1).

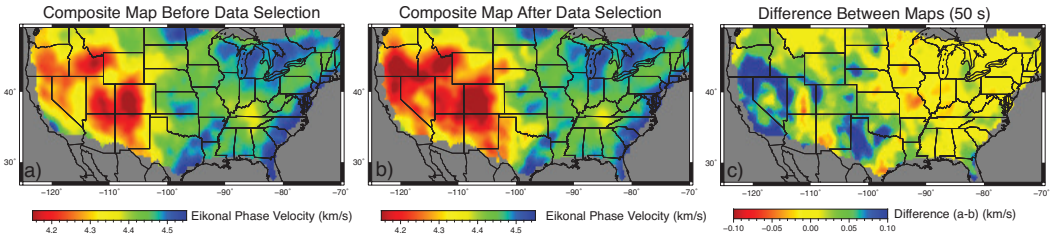

Figure 3. Illustration of the impact of quality control on 50-s Love wave phase velocity map. a) No data selection based on group arrival time difference ΔT. b) With data selection based on group arrival time difference ΔT. c) Difference, with (b) subtracted from (a). Positive values indicate faster velocity in (a).

4 Results: Composite Phase Velocity Maps

We present the final phase velocity maps made using our quality control approach in Fig. 4. At short periods ($T \leq 40$s), our maps can be compared to the USANT15 phase velocity maps derived from ambient noise (Ekström, 2017). We observe very strong agreement between the two models at periods of 35 and 40 s (Fig. S3), with an average absolute difference of ≈ 0.03 km/s.

The distributed depth-sensitivity of Love wave phase velocity measurements renders it impossible to interpret Love wave phase velocity anomalies in terms of shear velocity at specific depths. Nonetheless, the heterogeneity in our Love wave maps exhibits correlations with specific tectonic features (labeled in Fig. S4). At short periods ($T \leq$ 45 s), our measurements are very sensitive to crustal structure. At these periods, the lowest velocity anomalies occur along and south of the Southern Rocky Mountains. These low velocities extend northward along the Central Rocky Mountains and are lowest at the eastern tip of the Snake River Plain. In a slight difference from the maps of Foster, Ekström, and Nettles (2014), we also observe low velocities along the Cascades Range. Moderately low velocities are present along the Sierra Nevada Range and the eastern edge of the Great Basin, producing a 'ring' around the Basin and Range. In the eastern half of the U.S., the lowest phase velocity anomalies are located at the boundary between Kentucky and Tennessee. Many of the aforementioned zones of relatively low velocity are co-located with anomalously thick crust (Shen & Ritzwoller, 2016). At these short periods, the highest phase velocity values are located near and also along the Eastern Gulf

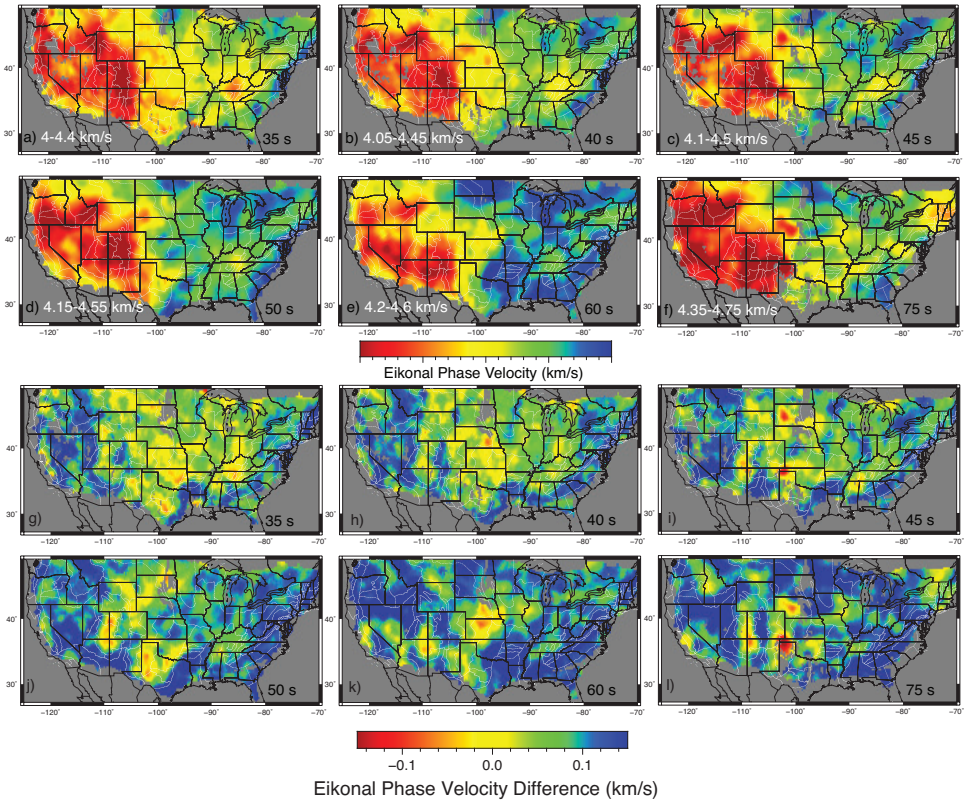

Figure 4. (a-f) New Love wave phase velocity maps, generated with data that meet our quality control approach. The period corresponding to each map is noted below at the bottom-right corner of each subplot, and the phase velocity range of the colorbar is shown on the bottom left. Pixels shown in gray had measurements from five or fewer events after quality control. Overlain on each map as white lines are physiographic provinces (after Fenneman (1928)). (g-l) Differences between our measured Love wave phase velocity maps and the phase velocity maps predicted using the isotropic shear velocity model SR16 (Shen & Ritzwoller, 2016); predicted phase velocities are subtracted from measured phase velocities.

Coastal Plain and also at the border of North Dakota and Minnesota, potentially related to the Superior Craton.

At longer periods ($T \geq 50$ s), the locations of the lowest velocity anomalies are shifted slightly relative to shorter periods. A prominent anomaly exists beneath the Colorado Plateau rather than the Southern Rocky Mountains, and at 60 and 75 s, one of the lowest-velocity anomalies parallels the border between California and Nevada, slightly east of the Sierra Nevada Range. As at shorter periods, we find a low-velocity anomaly along the Snake River Plain. In the eastern U.S., a zone of slightly low velocities is north-

west of the Blue Ridge province in the period range 45–60 s. At 75 s, we observe distinct low-velocity anomalies that correspond to the locations of the New England Upwelling (Levin et al., 2018) and the Reelfoot Rift, neither of which appear at shorter periods.

We quantify uncertainty in our maps by calculating the standard deviation of all the measurements at each pixel retained after quality control (Fig. S5). At all periods, the average uncertainty across all pixels is less than 0.2 km/s.

5 Discussion

5.1 Effects of Our Quality-Control Approach and Implications for Overtone Interference Globally

Even within the U.S., there are spatial variations in the degree to which a Love wave data set is biased by overtone interference and the effect of our quality control scheme on the features in phase-velocity maps (Fig. 3). This is due to factors like a station's location relative to the geographic distribution of earthquake sources as well as lateral variations in seismic velocity. In this section we conduct a simple experiment to explore the range in ΔT values and the extent of Love wave overtone interference at different locations on the Earth.

We divide the Earth's surface into pixels and assume that every pixel records all earthquakes in the Global CMT catalog (Ekström et al., 2012) that occurred during 2014 and 2015 and had $M_w \geq 6$. For every source-pixel pair, we calculate ΔT by integrating the FM and first-overtone group velocity maps (Section 2.2) along the great-circle path. Each pixel is then characterized by a distribution of ΔT values, each representing the degree of overtone interference, with smaller ΔT indicating stronger interference. We summarize this distribution with a single value: the percentage of measurements at each pixel with ΔT value greater than 1.2× the period of interest, corresponding to our preferred quality control threshold for data selection.

Maps of this quantity (Fig. S6) show that the likelihood of measuring Love waves that are minimally affected by overtone interference depends strongly on where the measurements are made. Locations where interference-free measurements are likely correspond to source-receiver paths where a considerable fraction of the propagation length is through continental lithosphere, where the FM and overtone group velocities are reasonably well separated (Fig. 1a). Our analysis shows that, at all periods, these locations

tend to be in Europe, Northern Africa, and western Asia. Locations where overtone interference affects a high percentage of Love wave measurements include the Pacific Ocean, the southern half of the Indian Ocean, the western U.S., and the eastern half of Australia. In addition to these geographical variations, there is a tendency for more high-quality measurements to be possible at the shortest and longest periods analyzed ($T \leq 50$s and $T \geq 125$ s) because of the larger group-velocity separation between the FM and overtones. For example, a measurement on the east coast of the U.S. has a 75% chance of passing our quality control criterion at 50 s, but a 30% chance of doing so at 100 s.

This experiment explains the regional variations in overtone interference observed with our USArray measurements. Fig. 3 shows a larger difference in the average phase velocities estimated with and without quality control at pixels in the western U.S. than in the eastern U.S. This is consistent with the results in Fig. S6a, which shows that locations in the western U.S. are more likely to record contaminated measurements. Thus, the application of our quality control criterion will more strongly impact average phase velocity measurements in the western U.S.

5.2 Implications for Radial Anisotropy

Our Love wave phase velocity maps offer a new opportunity to study radial anisotropy in the North American lithosphere. Although a full inversion for depth-dependent shear velocity and radial anisotropy (e.g. Gao & Lekić, 2018) is beyond the scope of this study, here we examine how well a high-resolution model of isotropic shear velocity in the U.S. can explain our observations and where, if anywhere, radial anisotropy is required.

We use the shear velocity model of Shen and Ritzwoller (2016) (hereafter referred to as SR16) to test the null hypothesis that radial anisotropy is not required in the lithosphere beneath USArray. SR16 was developed from joint inversion of Rayleigh wave phase velocity and ellipticity and P-to-s receiver functions and thus constrains V_{SV}. We sample depth-dependent profiles from SR16 on an evenly spaced grid, prescribe that $V_{SH} = V_{SV}$ and also that the speeds of horizontally and vertically traveling P waves are equal, $V_{PH} = V_{PV}$, and use MINEOS to predict Love wave phase velocity, with details as described by Babikoff and Dalton (2019). We test end-member scenarios for depth-dependent attenuation and find that realistic attenuation variations have a negligible impact on the predicted Love wave phase-velocity maps and our conclusions about radial anisotropy.

Fig. 4g-4l plots the difference between our Love wave phase velocity maps (Fig. 4a-4f) and the predictions from SR16. In the following discussion we assume that difference values not equal to zero indicate failure of our assumption of isotropy, $V_{SH} = V_{SV}$. The alternative option– that the lithosphere is isotropic but SR16 inadequately captures the seismic structure– is unlikely, since numerous other studies have produced models of V_{SV} that agree well with SR16 (Zhou et al., 2022; Netto et al., 2019), and Babikoff and Dalton (2019) found good agreement between their observed Rayleigh wave phase velocity maps and predictions of SR16. Nonetheless, a future 3-D inversion for radial anisotropy will carefully consider such a scenario.

We find that even after we have suppressed the bias to higher phase velocities due to overtone interference, at many locations our Love wave phase velocities are higher than the predictions. At short periods, these higher-than-predicted phase velocities are mostly distributed in the western and southeastern U.S. and closely follow the distribution of thin crust in the SR16 model. At long periods, higher-than-predicted phase velocities are found in most of the U.S.

In the western U.S., Moschetti et al. (2010) imaged crustal radial anisotropy using Love wave measurements from ambient noise at short periods ($T \leq 32$ s), and Rayleigh wave measurements in the period band (6 s $\leq T \leq$ 100 s). They found widespread positive radial anisotropy ($V_{SH} > V_{SV}$) in the middle-lower crust, and showed that this radial anisotropy was confined to provinces that underwent extension in the Cenozoic. This is consistent with our observations, particularly at 40 s, 45 s, and 50 s. At these periods, we find higher-than predicted phase velocities in the Basin and Range Province and north of the Snake River Plain, coincident with regional extension (Moschetti et al., 2010). On the other hand, regions not traditionally associated with extension, such as the Colorado Plateau, the Sierra Nevada Range, the Snake River Plain, and the Columbia Plateau in Oregon, do not show higher-than-predicted velocities and positive radial anisotropy in our images. At longer periods ($T > 50$ s), there is a reorganization in the patterns of phase velocity differences, and we instead observe higher-than-predicted phase velocities along the Snake River Plain and west of the Colorado Plateau, potentially suggestive of a change in the patterns of radial anisotropy at subcrustal depths.

We observe different behavior in the central and eastern U.S. Here, at periods $\leq$ 45 s, Love wave phase velocities agree much more closely with predictions from the isotropic

model, particularly at longitudes east of -105°. More broadly, this hints that radial anisotropy may not be ubiquitous in continental crust, as has been suggested (Dalton & Gaherty, 2013). In the eastern U.S., we observe regions of higher-than-predicted phase velocities to the southeast of the Blue Ridge province, in the Appalachian Highlands. At longer periods, we observe low differences in the central U.S. and in the vicinity of the New England Upwelling, as well as higher-than-predicted velocities along the Blue Ridge province.

We conclude by emphasizing that the differences in observed and predicted phase velocity (Fig. 4g-l) are similar in magnitude to the differences between Love wave phase velocity maps that are and are not corrected for overtone interference (Fig. 3). This emphasizes the importance of correcting for overtone-interference effects in order to accurately resolve radial anisotropy.

6 Conclusion

We present an approach to eliminate overtone interference in regional Love wave phase velocity measurements, and we apply it to measurements made at EarthScope USArray stations. By isolating measurements with a large group arrival time separation between the fundamental mode and the first overtone, we show that we are able to eliminate three sources of contamination due to overtone interference: elevated scatter in phase velocity measurements, a systematic bias to anomalously high velocity, and oscillation as a function of epicentral distance. Although the focus of this study is the U.S., we also quantify how 3-D velocity heterogeneity and the global distribution of earthquake sources produce geographic variability around the globe in the likelihood that a Love wave measurement is contaminated by overtone interference.

Using the quality-controlled USArray data set, we present Love wave phase velocity maps spanning the conterminous U.S. in the period range 35–75 seconds. We observe correlations with known physiographic features. By comparing our maps to predictions of an isotropic shear velocity model, we show that radial anisotropy is required in the upper mantle beneath much of the U.S. and in the crust of the western U.S. However, predictions from the isotropic model can explain the Love wave phase velocities at shorter periods throughout the central U.S.

Open Research Section

The phase velocity maps developed in the study are available at the Brown University Digital Repository via https://doi.org/10.26300/2sy8-tk50 and also in the suppplementary information. The waveform data used to make phase-delay measurements can be downloaded from the IRIS Data Management Center.

Acknowledgments

We thank Göran Ekström for sharing Love wave USArray measurements and making his ambient noise tomographic model available on his website: https://www.ldeo.columbia.edu/~ekstrom/Projects/ANT/USANT15/. We thank Jordyn Babikoff for assistance with MINEOS calculations. This work was supported by the U.S National Science Foundation under grants EAR-1553367 and EAR-1829401 to C.A.D., and by an NSF Graduate Research Fellowship (DGE-16-44760) to A.H. Some figures were made with the Generic Mapping Tools (Wessel et al., 2019). The tomographic models CSEM-NA, SAVANI-US and Y14 were downloaded from the IRIS Earth Model Collaboration (EMC), accessible at https://ds.iris.edu/ds/products/emc-csem_north_america/, http://ds.iris.edu/ds/products/emc-savani_us/ and http://ds.iris.edu/ds/products/emc-semum_na14/ respectively. The Earth model Z22 was downloaded from https://labs.utdallas.edu/seismic-imaging-lab/download/.

References

Babikoff, J. C., & Dalton, C. A. (2019). Long period Rayleigh wave phase velocity tomography using USArray. *Geochemistry, Geophysics, Geosystems*.

Babuska, V., & Cara, M. (1991). *Seismic anisotropy in the earth* (Vol. 10). Springer Science & Business Media.

Becker, T. W., Kustowski, B., & Ekström, G. (2008). Radial seismic anisotropy as a constraint for upper mantle rheology. *Earth and Planetary Science Letters*, *267*(1-2), 213–227.

Dalton, C. A., & Gaherty, J. B. (2013). Seismic anisotropy in the continental crust of northwestern canada. *Geophysical Journal International*, *193*(1), 338–348.

Eddy, C. L., & Ekström, G. (2014). Local amplification of Rayleigh waves in the continental United States observed on the USArray. *Earth and Planetary Science Letters*, *402*, 50–57.

Eddy, C. L., & Ekström, G. (2020). Comparisons between measurements and predictions of Rayleigh wave amplification across the contiguous United States. *Physics of the Earth and Planetary Interiors*, *299*, 106407.

Eddy, C. L., Ekström, G., & Nettles, M. (2022). Three-dimensional seismic anisotropy in the pacific upper mantle from inversion of a surface-wave dispersion dataset. *Geophysical Journal International*.

Ekström, G. (2011). A global model of Love and Rayleigh surface wave dispersion and anisotropy, 25-250 s. *Geophysical Journal International*, *187*(3), 1668–1686.

Ekström, G. (2017). Short-period surface-wave phase velocities across the conterminous united states. *Physics of the Earth and Planetary Interiors*, *270*, 168–175.

Ekström, G., Nettles, M., & Dziewoński, A. (2012). The global CMT project 2004–2010: Centroid-moment tensors for 13,017 earthquakes. *Physics of the Earth and Planetary Interiors*, *200*, 1–9.

Ekström, G., Tromp, J., & Larson, E. W. (1997). Measurements and global models of surface wave propagation. *Journal of Geophysical Research: Solid Earth*, *102*(B4), 8137–8157.

Fenneman, N. M. (1928). Physiographic divisions of the united states. *Annals of the Association of American Geographers*, *18*(4), 261–353.

Foster, A., Ekström, G., & Nettles, M. (2014). Surface wave phase velocities of the Western United States from a two-station method. *Geophysical Journal International*, *196*(2), 1189–1206.

Foster, A., Nettles, M., & Ekström, G. (2014). Overtone interference in array-based Love-wave phase measurements. *Bulletin of the Seismological Society of America*, *104*(5), 2266–2277.

Gao, C., & Lekić, V. (2018). Consequences of parametrization choices in surface wave inversion: Insights from transdimensional bayesian methods. *Geophysical Journal International*, *215*(2), 1037–1063.

Hariharan, A., Dalton, C. A., Babikoff, J., & Ekström, G. (2022). Controls on surface wave overtone interference. *Geophysical Journal International*, *228*(3), 1665–1683.

James, E. K., Dalton, C. A., & Gaherty, J. B. (2014). Rayleigh wave phase velocities

in the Atlantic upper mantle. *Geochemistry, Geophysics, Geosystems*, *15*(11), 4305–4324.

Jin, G., & Gaherty, J. B. (2015). Surface wave phase-velocity tomography based on multichannel cross-correlation. *Geophysical Journal International*, *201*(3), 1383-1398. Retrieved from +http://dx.doi.org/10.1093/gji/ggv079 doi: 10.1093/gji/ggv079

Karato, S.-i., & Park, J. (2018). On the origin of the upper mantle seismic discontinuities. *Lithospheric discontinuities*, 5–34.

Kustowski, B., Ekström, G., & Dziewoński, A. (2008). Anisotropic shear-wave velocity structure of the Earth's mantle: A global model. *Journal of Geophysical Research: Solid Earth*, *113*(B6).

Laske, G., Masters, G., Ma, Z., & Pasyanos, M. (2013). Update on crust1. 0—a 1-degree global model of earth's crust. In *Geophysical research abstracts* (Vol. 15, p. 2658).

Levin, V., Long, M. D., Skryzalin, P., Li, Y., & López, I. (2018). Seismic evidence for a recently formed mantle upwelling beneath new england. *Geology*, *46*(1), 87–90.

Lin, F.-C., & Ritzwoller, M. H. (2011). Helmholtz surface wave tomography for isotropic and azimuthally anisotropic structure. *Geophysical Journal International*, *186*(3), 1104–1120.

Lin, F.-C., Ritzwoller, M. H., & Snieder, R. (2009). Eikonal tomography: surface wave tomography by phase front tracking across a regional broad-band seismic array. *Geophysical Journal International*, *177*(3), 1091–1110.

Masters, G., Woodhouse, J. H., & Freeman, G. (2011). *Mineos v1.0.2.* Retrieved from https://geodynamics.org/cig/software/mineos/

Moschetti, M., Ritzwoller, M., Lin, F.-C., & Yang, Y. (2010). Seismic evidence for widespread western-us deep-crustal deformation caused by extension. *Nature*, *464*(7290), 885–889.

Nettles, M., & Dziewoński, A. M. (2011). Effect of higher-mode interference on measurements and models of fundamental-mode surface-wave dispersion. *Bulletin of the Seismological Society of America*, *101*(5), 2270–2280.

Netto, A., Pulliam, J., & Persaud, P. (2019). Synoptic view of lithospheric s-wave velocity structure in the southern united states: A comparison of 3d seismic

tomographic models. *GSA Today*, *29*(7).

Ribe, N. M. (1992). On the relation between seismic anisotropy and finite strain. *Journal of Geophysical Research: Solid Earth*, *97*(B6), 8737–8747.

Rohde, M. D., Ringler, A. T., Hutt, C. R., Wilson, D. C., Holland, A. A., Sandoval, L., & Storm, T. (2017). Characterizing local variability in long-period horizontal tilt noise. *Seismological Research Letters*, *88*(3), 822–830.

Selway, K., Ford, H., & Kelemen, P. (2015). The seismic mid-lithosphere discontinuity. *Earth and Planetary Science Letters*, *414*, 45–57.

Shen, W., & Ritzwoller, M. H. (2016). Crustal and uppermost mantle structure beneath the United States. *Journal of Geophysical Research: Solid Earth*, *121*(6), 4306–4342.

Thatcher, W., & Brune, J. N. (1969). Higher mode interference and observed anomalous apparent Love wave phase velocities. *Journal of Geophysical Research*, *74*(27), 6603–6611.

Wessel, P., Luis, J., Uieda, L., Scharroo, R., Wobbe, F., Smith, W. H., & Tian, D. (2019). The generic mapping tools version 6. *Geochemistry, Geophysics, Geosystems*, *20*(11), 5556–5564.

Zhou, T., Xi, Z., Chen, M., & Li, J. (2022). Assessment of seismic tomographic models of the contiguous united states using intermediate-period 3-d wavefield simulation. *Geophysical Journal International*, *228*(2), 1392–1409.

Zürn, W., Forbriger, T., Widmer-Schnidrig, R., Duffner, P., & Ringler, A. T. (2022). Modelling tilt noise caused by atmospheric processes at long periods for several horizontal seismometers at bfo—a reprise. *Geophysical Journal International*, *228*(2), 927–943.